# NRC Publications Archive
# Archives des publications du CNRC

**Functionally graded cathode catalyst layers for polymer electrolyte fuel cells. I, Theoretical modeling**

Wang, Qianpu; Eikerling, Michael; Song, Datong; Liu, Zhongsheng; Navessin, Titichai; Xie, Zhong; Holdcroft, Steven

# Functionally Graded Cathode Catalyst Layers for Polymer Electrolyte Fuel Cells

## I. Theoretical Modeling

**Qianpu Wang,[a] Michael Eikerling,[a,b] Datong Song,[a] Zhongsheng Liu,[a,z] Titichai Navessin,[a,b] Zhong Xie,[a] and Steven Holdcroft[a,b]**

[a]*Institute for Fuel Cell Innovation, National Research Council Canada, Vancouver, British Columbia V6T 1W5, Canada*

[b]*Department of Chemistry, Simon Fraser University, Burnaby, British Columbia V5A 1S6, Canada*

The effect of Nafion loading on the electrode polarization characteristics of a proton exchange membrane fuel cell is studied with a macrohomogeneous model. The composition dependence of performance is rationalized by first relating mass fractions of the different components to their volume fractions and thereafter involving concepts of percolation theory to parameterize effective properties of the cathode catalyst layers. In particular, we explore systematically the effect of Nafion content on the performance. For a uniform layer, the best performance is obtained with a Nafion content of about 35 wt %, representing an optimum balance of proton transport, oxygen diffusion, and electrochemically active surface area. With the help of this modeling tool, we propose a nonuniform Nafion catalyst layer and the modeling indicates that such a layer improves performance. Our preliminary experiments (to appear in Part II) confirm this claim. The two cases of nonuniform Nafion distribution across the entire thickness include: a three-sublayer structure with equally thick layers, simulating a constant gradient, and a two-sublayer structure with variable thickness of the sublayers. Compared with the optimum Nafion content (35 wt %) in uniform distribution, the three-sublayer structure with higher Nafion content on the membrane side exhibits significantly enhanced performance.
© 2004 The Electrochemical Society. [DOI: 10.1149/1.1753580] All rights reserved.

Despite enormous improvements, major voltage losses in polymer electrolyte fuel cells (PEFCs) are still due to the poor kinetics of the oxygen reduction reaction (ORR) and transport limitations of protons and reactants in cathode catalyst layers. The kinetics of ORR at platinum/polymer electrolyte interfaces has been investigated extensively for several decades[1-8] with the objective of improving catalyst efficiency and reducing voltages losses.[9,10] High efficiencies for ORR with electrodes containing low platinum loadings have been achieved by incorporating Nafion ionomer into the matrix of carbon-supported Pt/C.[11-13]

Cathode catalyst layers in PEFCs are thin films sandwiched between membranes and gas diffusion layers (GDL, carbon paper or carbon cloth). The major ingredients of catalyst layers are Nafion and Pt/carbon black. The common methods of preparation, including brushing, printing, and spray deposition followed by drying, lead to a porous microstructure. The distribution of ingredients and the fabrication process dictate the distribution of pores and networks, which form the pathways of reactant transport to the three-phase boundaries where the electrochemical reactions take place.

Many experimental studies have been performed on the optimization of the catalyst layer composition.[9,14-23] The study by Uchida *et al.*[15,16] focused on the role of the gas-supplying network. Lee *et al.*[18] evaluated the effect of Nafion loading on charge-transfer resistance and mass transport. Recently, Antolini *et al.*[19] and Passalacqua *et al.*[23] determined an optimum Nafion content of 33-40 wt %. Experimental findings suggest that Nafion primarily fills macropores, thereby increasing the Pt|ionomer contact area and improving proton conductivity.[15,16] At high Nafion loading, however, extensive blocking of macropore space results in diminishing both the rate of oxygen supply and the rate of water removal.

The purpose of this work is to further understand the role of Nafion in fuel cell catalyst layers. This is achieved by exploring a macrohomogeneous modeling approach, which relates the contents of C, Pt, and Nafion to the current-voltage characteristics. An attempt to theoretically rationalize the experimentally observed composition dependence was first described in Ref. 8 and 24 based on a two-phase balance of electrolyte and gas pores within preformed void space within the carbon/catalyst matrix. Following this, the full interplay between volume portions of ionomer, carbon/catalyst, and pores was considered in Ref. 25, using concepts of percolation theory.

In this work, we first establish relations between weight fractions and volume fractions. Thereafter, the effect of Nafion loading on the electrode performance is rationalized using the macrohomogeneous model.[8,26-30] After determining the optimum Nafion content of a uniform catalyst layer as a baseline, alternative design options using nonuniform distributions of Nafion are systematically explored.

## Model Description

For modeling purposes, the cathode catalyst layer (CL) is assumed to consist of a matrix of carbon and catalyst platinum, with ionomer electrolyte and pore space distributed homogeneously within. The microstructure of the catalyst layer, which identifies the distinct solid phases and gas pores, is shown in Fig. 1a. The spatial coordinate $x$ is defined in Fig. 1, with positive direction pointing from the gas GDL|CL interface toward the membrane. Protons diffuse into the catalyst layer from the membrane side on the right and oxygen diffuses into the layer from the GDL on the left. On the surfaces of finely dispersed catalyst particles, oxygen is consumed together with protons, producing liquid water along with waste heat. The cathodic half-reaction is

$$4H^+ + 4e^- + O_2 \rightarrow 2H_2O \qquad [1]$$

The dissolution of oxygen in the electrolyte is considered to be a fast process. The local concentration of oxygen in the electrolyte is assumed to be proportional to the gas-phase oxygen concentration in the same local volume element, determined by Henry's law. The product water is assumed to be removed efficiently. The oxygen flux, $N_{O_2}$, through the catalyst layer is assumed to be driven by a concentration gradient. It is thus determined by Fick's law of diffusion

$$\frac{dc_{O_2}}{dx} = -\frac{N_{O_2}}{D_{O_2}^{eff}} \qquad [2]$$
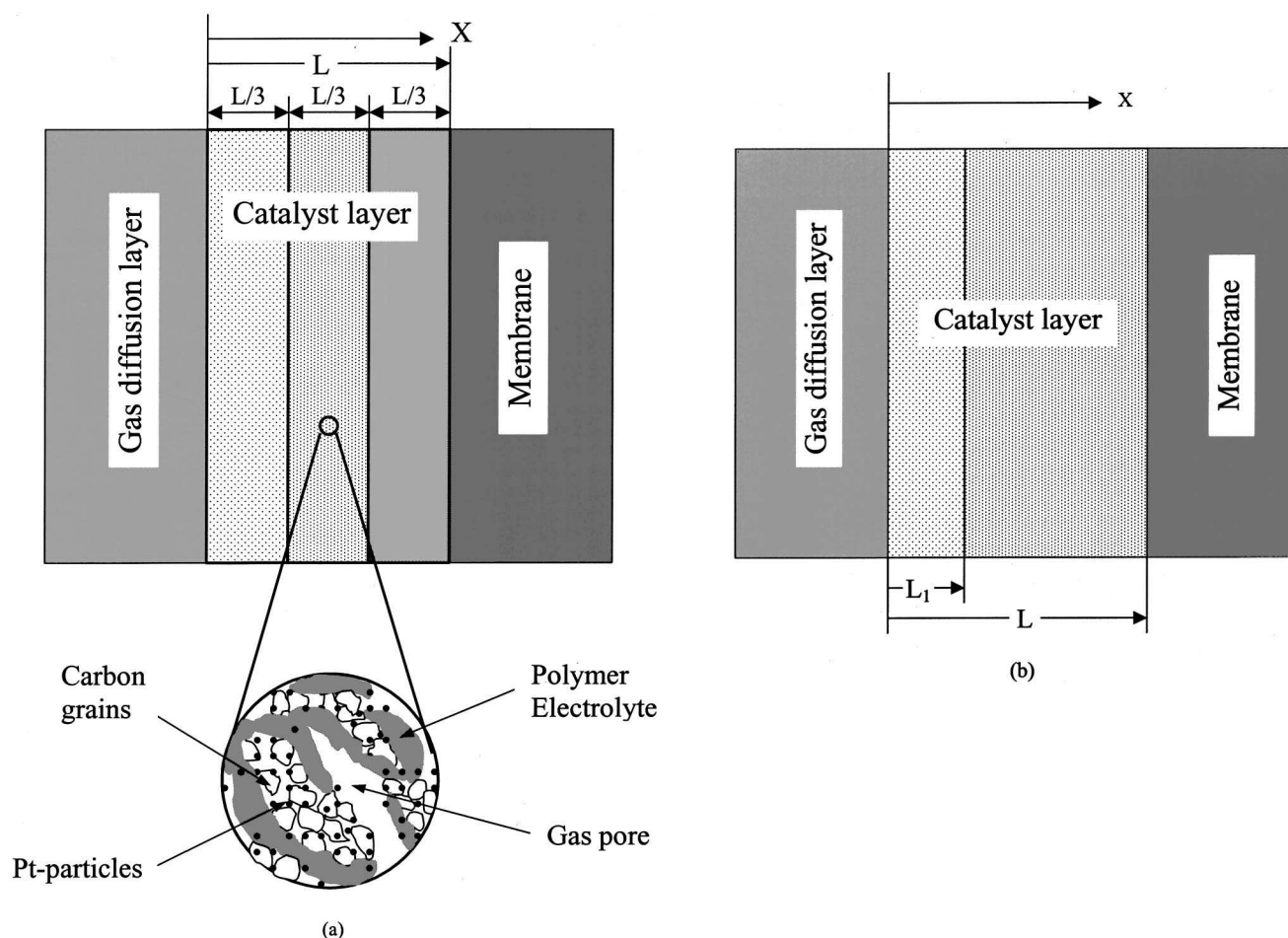
with

**Figure 1.** Schematic picture of the of cathode catalyst layer with nonuniform composition: (a) three-sublayer design with "constant" Nafion gradient and (b) two-sublayer design with nonconstant Nafion gradient.

$$N_{O_2}(x) = -\frac{j(x) - I_0}{4F} \qquad [3]$$

Here, $c_{O_2}$ represents the oxygen concentration, $D_{O_2}^{eff}$ is an effective oxygen diffusion constant, $j(x)$ is the local proton current density, and $I_0$ is the total current density through the cell.

Ohmic losses due to electronic transport are neglected, assuming a good conductivity of the carbon/catalyst phase. The Pt/C phase is thus considered to be equipotential, $\phi_m = 0$. The local electrode potential, $\eta(x)$, defined as the difference in electrical potentials between metal phase (Pt/C) and electrolyte phase, is thus solely determined by the local electrolyte potential, $\eta(x) = \phi_s - \phi_m = \phi_s(x)$. Proton migration in the ionomer phase can be described by Ohm's law

$$\frac{d\eta(x)}{dx} = \frac{j(x)}{\sigma^{eff}} \qquad [4]$$

$\sigma^{eff}$ is the effective ionic conductivity of the layer.

The boundary conditions are

$$x = 0 \quad j(x = 0) = 0 \quad c_{O_2} = c_{O_2}^* \qquad [5]$$

$$x = L \quad j(x = L) = I_0 \quad \frac{dc_{O_2}}{dx} = 0 \qquad [6]$$

which express that the oxygen flux is zero at the catalyst layer/membrane interface and the oxygen concentration at the GDL|CL interface is $c_{O_2}^*$.

The ORR kinetics follows Tafel law and is of first order in oxygen concentration[4]

$$\frac{dj(x)}{dx} = S_a^{eff} i_0^{ref} \left[ \left( \frac{c_{O_2,l}}{c_0^{ref}} \right) \exp\left( \frac{\alpha_c F}{RT} \eta(x) \right) \right.$$
$$\left. - \exp\left( -\frac{(1 - \alpha_c)F}{RT} \eta(x) \right) \right] \qquad [7]$$

where $c_0^{ref}$ is the reference oxygen concentration and $i_0^{ref}$ is the reference exchange current density, $S_a^{eff}$ is the electrochemically active Pt|ionomer contact area per unit volume, and $c_{O_2,l}$ is the dissolved oxygen concentration in the electrolyte, determined by Henry's law[26]

$$c_{O_2,l} = c_{O_2}/K_{O_2} \qquad [8]$$

$K_{O_2}$ is Henry's constant for oxygen gas dissolution in the ionomer. It is calculated from the empirical relation[28-30]

$$K_{O_2} = \frac{1}{RT} \exp\left( -\frac{666}{T} + 14.1 \right) \qquad [9]$$

**Table I. The base-case conditions and physical properties.**

| Parameter | Value |
|---|---|
| The platinum surface area per unit mass of the platinum, $A_s$ | 1120 cm²/mg |
| Oxygen concentration on the interface of GDL and catalyst layer, $c_{O_2}^*$ | $7.9239 \times 10^{-6}$ mol/cm³ |
| Oxygen reference concentration, $c_0^{ref}$ | $1.2 \times 10^{-6}$ mol/cm³ |
| Residual diffusivity, $d$ | $1 \times 10^{-4}$ |
| Bulk oxygen diffusion coefficient, $D_{O_2}$ | 0.2585 cm²/s |
| Reference exchange current density, $i_0^{ref}$ | $1.3183 \times 10^{-9}$ A/cm² |
| Catalyst layer thickness, $L$ | $1.8 \times 10^{-3}$ cm |
| Platinum loading in the catalyst layer, $m_{Pt}$ | 0.42 mg/cm² |
| Cell temperature, $T$ | 323 K |
| Percolation threshold, $X_0$ | 0.1 |
| Platinum mass fraction on carbon black, $Y_{Pt}$ | 20% |
| Density of carbon, $\rho_C$ | $2 \times 10^3$ mg/cm³ |
| Density of platinum, $\rho_{Pt}$ | $2.15 \times 10^4$ mg/cm³ |
| Density of electrolyte (Nafion), $\rho_{el}$ | $1.9 \times 10^3$ mg/cm³ |
| Proton bulk conductivity, $\sigma_s$ | 0.07 S/cm |
| Cathode transfer coefficient, $\alpha_c$ | 0.75 |

Three effective parameters $D_{O_2}^{eff}$, $\sigma^{eff}$, and $S_a^{eff}$ are determined by the volume fractions of the catalyst layer components, which are discussed in the next section.

### Percolation Properties

Parameterizations of catalyst layer properties as functions of composition refer to the class of percolation problems, cf. Ref. 8, 24-28,31,32. The percolation model was discussed by Hammersley[33] in 1957 and has since found numerous applications. Here we employ the percolation model proposed in Ref. 8 and 25 for the cathode catalyst layer.

The effective proton conductivity is determined by the volume fraction of the ionomer electrolyte, expressed as[8,24]

$$\sigma^{eff} = \sigma_s \frac{(X_{el} - X_0)^\tau}{(1 - X_0)^\tau} \Theta(X_{el} - X_0) \qquad [10]$$

where $\sigma_s$ is the bulk proton conductivity; $\tau$ is the critical exponent, $\tau \approx 2$,[34-36]; $\Theta$ is the Heaviside step function, which accounts for zero conductivity below the percolation threshold; $X_0$ is the percolation threshold; and $X_{el}$ is the volume portion of the electrolyte.

Consideration of oxygen transport in the catalyst layer is more complex. Oxygen transports to the reaction sites in two ways: gas phase diffusion through a percolation cluster of gas pores and residual diffusion of dissolved oxygen through ionomer electrolyte. The bulk diffusion coefficient in the gas channel is larger than in the electrolyte by a factor of $10^4$-$10^5$. The latter is considered by a residual diffusivity, and the effective diffusion coefficient can be expressed as,[8,24,25,34,35]

$$D_{O_2}^{eff} = \frac{D_{O_2}}{(1 - X_0)^\tau + d}[(1 - X_{Pt} - X_C - X_{el} - X_0)^\tau \Theta$$
$$\times (1 - X_{Pt} - X_C - X_{el} - X_0) + d] \qquad [11]$$

where $D_{O_2}$ is the bulk oxygen diffusion coefficient. The coefficient $d$ accounts for the resident diffusivity due to diffusion through micropores or polymer materials as these pathways remain intact, if even all macropores are blocked by electrolyte. $X_{Pt}$ is the volume fraction of platinum and $X_C$, the volume fraction of carbon. The volume fraction of the remaining open pore space is then given by $X_V = 1 - X_{Pt} - X_C - X_{el}$. The critical exponent of diffusion, $\tau$, is universal for standard lattice percolation.[35] Values of $\tau \approx 2$ are suggested in three dimensions by theoretical studies. However, we are aware that for specific structures, including fibrous structures[32]



(a)


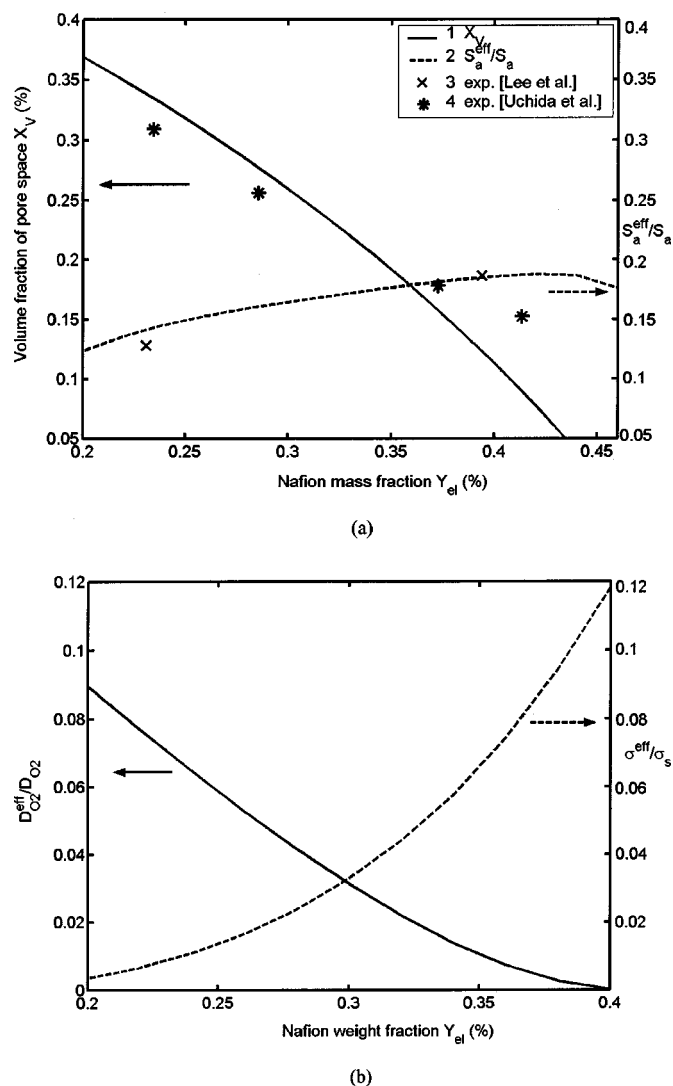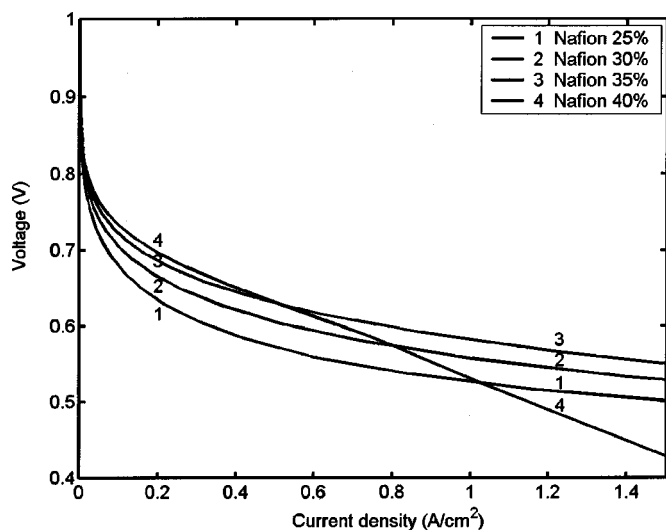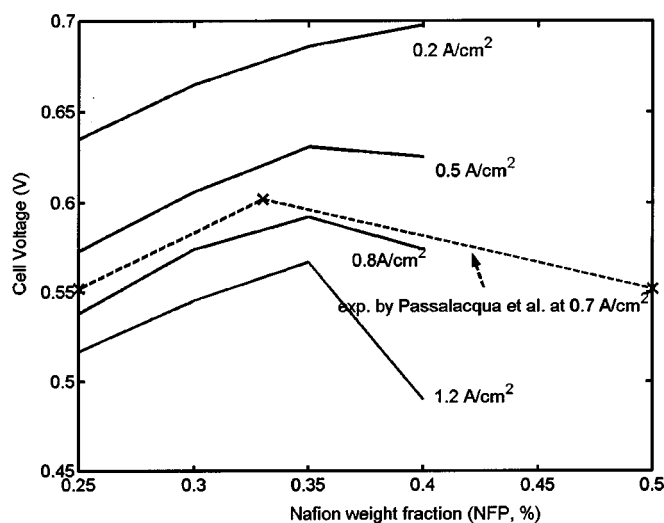
(b)

**Figure 2.** Dependence of catalyst layer parameters on Nafion weight fraction: (a) comparison of volume fraction of pore space $X_V$ and electrochemically active surface area ($S_a^{eff}/S_a$) with experimental data[15-16,18] and (b) oxygen diffusion coefficient ($D_{O_2}^{eff}/D_{O_2}$) and effective proton conductivity ($\sigma^{eff}/\sigma_s$) (no experimental measurement available).

(a)



(b)

**Figure 3.** Dependence of catalyst layer performance on Nafion weight fraction for uniform layers: (a) I-V plots of the catalyst layer and (b) cell potential as a function of Nafion weight fraction for different current densities. Experimental data[23] are shown for comparison. The experimental data have been corrected for the membrane contribution, displaying only the contribution of the cathode catalyst layer to the fuel cell voltage.

and for distinct types of continuum percolation models, *e.g.*, the so-called Swiss cheese model,[37] different critical exponents could be found. However, in view of the yet unresolved structural picture of CL we believe that $\tau \approx 2$ is a reasonable choice, because it apparently can be used for a broad class of random heterogeneous structures.

The platinum electrochemical active area is the specific area of the Pt/ionomer interface which is accessible for protons as well as for oxygen and it depends on the volume fractions of Pt/C, electrolyte, and pore space. It is logical to adopt a parameterization that rests on the theory of active bonds in dual porous composite materials[25] so that

$$S_a^{eff} = S_a \{ P(X_{el}) P(X_{Pt} + X_C) \lfloor (1 - \chi)(1 - [1 - P(X_V)]^M) $$
$$+ \chi [1 - P(X_V)]^M ] \} \qquad [12]$$

**Table II. Influence of Nafion loading on fuel-cell performance, comparison of modeling and experimental data.**

| Reference | Conditions | | Optimum Nafion content wt % |
| | Pt/C wt % | Pt loading (mg/cm²) | |
|---|---|---|---|
| Modeling, this work | 20 | 0.42 | 35 |
| Exp. by Uchida *et al.*[15] | 25 | 2 | 33 |
| Exp. by Paganin *et al.*[17] | 10 | 4 | 30-35 |
| Exp. by Antolini *et al.*[19] | 20 | 1 | 40 |
| Exp. by Passalacqua *et al.*[23] | 20 | 0.5 | 33 |

Here, $S_a$ is the total specific platinum area (in cm²/cm³), proportional to the platinum loading and catalyst layer thickness, which can be expressed by

$$S_a = A_s \frac{m_{Pt}}{L} \qquad [13]$$

where $m_{Pt}$ is the platinum loading and $A_s$ is the platinum surface area per unit mass of the platinum. $\chi$ accounts for the residual electrochemical active area of fully flooded domains in the catalyst layer. The factor $P(X_{el})P(X_{Pt} + X_C)$ in Eq. 12 takes into account the probability of an interface between a carbon/catalyst and an electrolyte particle with both of them connected to their corresponding infinite clusters. $P(X)$ is the density of an infinite cluster of a percolating component, determined by[25]

$$P(X) = \frac{X}{[1 + \exp[-a(X - X_0)]]^b} \qquad [14]$$

with $a = 53.7$, $b = 3.2$, and the parameter $M$ is the average number of bond neighbors ($M = 4$).

## Constitutive Relations between Weight Fractions and Volume Fractions

From a statistical or mathematical modeling point of view, the effective properties are determined by the volume fractions of distinct components. By using percolation theory the effect of these volume fractions on proton conductivity, oxygen diffusion coefficient, and exchange current density can be rationalized. In experimental investigations, the composition is usually specified in terms of weight fractions, which are readily controlled during the fabrication process. It would, thus, be very useful to link the performance directly to the weight fractions of the catalyst layer components. The volume fractions of distinct components can be expressed via weight fractions, catalyst loading, and catalyst layer thickness using the following relations

$$X_V = 1 - \left[ \frac{1}{\rho_{Pt}} + \frac{1 - Y_{Pt}}{Y_{Pt}\rho_c} + \frac{Y_{el}}{(1 - Y_{el})Y_{Pt}\rho_{el}} \right] \frac{m_{Pt}}{L} \qquad [15]$$

$$X_{Pt} = \frac{m_{Pt}}{L} \frac{1}{\rho_{Pt}} \qquad [16]$$

$$X_C = \frac{m_{Pt}}{L} \frac{1 - Y_{Pt}}{Y_{Pt}\rho_C} \qquad [17]$$

$$X_{el} = \frac{m_{Pt}}{L} \frac{Y_{el}}{(1 - Y_{el})Y_{Pt}\rho_{el}} \qquad [18]$$

where $Y_{Pt}$ is the platinum mass fraction on the supported carbon black. $Y_{el}$ is the mass fraction of electrolyte (electrolyte loading), which is determined from the percentage of electrolyte and total catalyst weight using the following relation[19]

$$Y_{el}$$
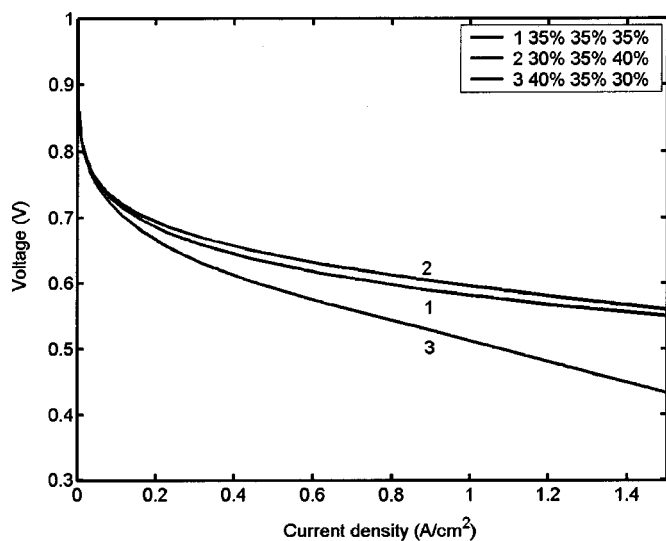
(a)
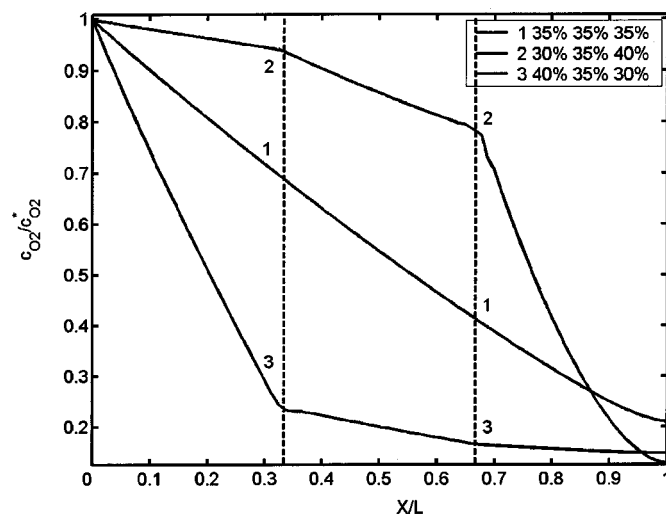


(b)

**Figure 4.** Performance dependence on Nafion weight fraction for nonuniform Nafion distributions in the catalyst layer (percent values refer to Nafion weight fraction in the sublayer): (a) catalyst layer polarization curves and (b) oxygen concentration profiles at 0.6 V. In the legend, percent values refer to Nafion content in the sublayer. GDL is to the left and membrane is to the right.

$$= \frac{\text{mg electrolyte cm}^{-2}}{(\text{mg electrolyte cm}^{-2}) + \text{mg Pt cm}^{-2} + \text{mg carbon cm}^{-2}} \quad [19]$$

Here, adopting the catalyst layer preparation method of impregnating Nafion into the electrode, we assume that the carbon and Pt phases form a solid matrix with an initial volume fraction of void space $X_V(Y_{el} = 0)$. The voids are either filled by Nafion or remain Nafion-free. It is assumed that Nafion can impregnate the void space without affecting the thickness of catalyst layer or its total volume.

### Results and Discussion

The set of governing differential equations, Eq. 2-4, was solved using MATLAB software.[38] The base-case conditions and physical properties are given in Table I.
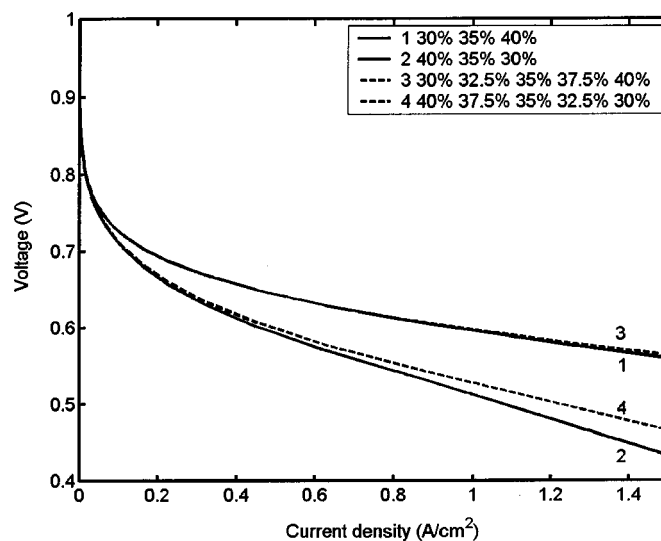


**Figure 5.** Comparison of the polarization curves for three- and five-sublayer structure.

*Parameterization of composition dependence.*—Based on Eq. 10-12, the dependencies of the elementary parameters on the electrolyte content can be determined. Figure 2a shows the resulting volume fraction of pore space and electrochemically active surface area (ESA) as functions of the Nafion weight fraction. The volume fraction of the pore space decreases with increasing $Y_{el}$. $S_a^{eff}$ goes up gradually with $Y_{el}$ and peaks at $Y_{el} = 43$ wt %; after that it falls slowly. In Fig. 2b, dependencies of the effective oxygen diffusion coefficient and effective proton conductivity on $Y_{el}$ are presented. The effective oxygen diffusion coefficient drops with an increase of $Y_{el}$, but there is an opposite trend in the proton conductivity. These data clearly reflect the competition between the three major parameters (proton transport, oxygen supply, and ESA).

The experimental studies relating the effects of $Y_{el}$ to the catalyst layer parameters have been presented by Uchida *et al.*[15,16] and Lee *et al.*[18] Uchida *et al.* prepared the electrode by directly mixing the ionomer with 25 wt % platinum-loaded carbon to form colloids, while Lee *et al.* impregnated the Pt/C catalyst layer with different loadings of solubilized Nafion, in a manner similar to the conditions assumed in our model. The specific pore volume (cm³/g) was measured for varying ionomer content by Uchida *et al.*, and active surface area (cm²/cm²) was measured by Lee *et al.* These data are reproduced in Fig. 2a. According to Uchida *et al.*, the volume of secondary pores (macropores of size 40-200 nm formed between agglomerates) decreases linearly with increase in $Y_{el}$, but that of the primary pores (micropores of size 20-40 nm formed within agglomerates) remains unchanged. Compared with experimental results by Uchida *et al.*, the predicted volume fraction by assuming constant thickness in a certain Nafion content range is in reasonable agreement. The ESA of the electrode was measured by cyclic voltammetry by Lee *et al.* The results show it increases with an increase in $Y_{el}$ up to 57.45 wt % Nafion. The theoretical result indicates that ESA decreases after the Nafion content exceeds 43 wt %. In the range of Nafion content between 20 and 40 wt %, the modeling is in reasonable agreement with experimental data. The adoption of parameterizations that rest on the theory of active bonds in dual porous composites (Eq. 12) is, thus, a reasonable approach to study composition-dependent physical properties of catalyst layers.

*Effect of Nafion content on performance.*—The dependence of catalyst layer performance on $Y_{el}$ for a uniform CL is illustrated in Fig. 3. The curves demonstrate that there is an upward trend in performance in relation to $Y_{el}$, and in the performance peaks at $Y_{el} = 35$ wt %, further increase in $Y_{el}$ enhances performance only at

lower current densities, for which oxygen diffusion is not rate limiting. In this range, larger values of $Y_{el}$ lead to a reduction of ohmic losses and thereby to improvement of the performance. At higher current density ($>0.5$ A/cm$^2$), increasing $Y_{el}$ above 35 wt % leads to the reduced performance because of its deleterious impact on oxygen diffusion.

The cell potential at several current densities is shown in Fig. 3b as a function of $Y_{el}$, and is compared with experimental data reported by Passalacqua *et al.*[23] In the model, only the catalyst layer was considered. The experimental data reported by Passalacqua *et al.* included the whole membrane electrode assembly (MEA). Therefore, an ohmic membrane contribution of 0.1225 V (Nafion 117 with thickness 175 μm and proton conductivity 0.1 S/cm) was added to the experimental data at 0.7 A/cm$^2$, so that only the effect of the cathode catalyst layer is displayed in Fig. 3b. The anodic overpotential is considered to be negligible. With this correction, Fig. 3b reveals good agreement between model results and experimental data. The same trend was reported by Uchida *et al.* Table II shows a comparison between the modeling results and the literature data. It was found that modeling results of optimal $Y_{el}$ are in the range of the literature data, particularly close to the results reported by Uchida *et al.* and Passalacque *et al.*

*Nafion gradient in catalyst layer design.*—The previous results demonstrated the competition between the three major parameters in the way that improving one parameter could lead to worsening of the other two. In order to further temper the distinct catalyst layer functions, we explore simple variants of functionally graded catalyst layer compositions. In this kind of design, the catalyst layer is processed as a sublayer structure with gradually varying composition. Two different options are investigated here: a three-sublayer structure with equally thick sublayers, simulating a linear gradient, and a two-sublayer with varying thickness of sublayers simulating a nonlinear gradient. The selection of the distinct sublayer structures was made in view of their possible practical fabrication. A simple way is to deposit additional Nafion into existing impregnated catalyst layers. The Nafion solution penetrates to a certain depth, which can establish Nafion gradient in two-sublayer structures.

*Three-sublayer structure ("constant" gradient).*—The catalyst layer is divided into three sublayers of identical thickness, shown in Fig. 1a. Three combinations of $Y_{el}$ are investigated. From the calculation described previously, the optimum $Y_{el}$ for homogeneous catalyst layer is 35 wt %; this is chosen as the baseline $Y_{el}$. Figure 4a shows the effect of different Nafion distributions on the polarization curves. Case 1 is the baseline-homogeneous case, in which the volume fraction of void spaces is about 19%. In case 2, $Y_{el}$ is 30 wt % on the GDL side, 35 wt % in the middle, and 40 wt % on the membrane side, in which the volume fractions of void spaces in the sublayers are about 26% (GDL side), 19% (middle), and 12% (membrane side). Case 3 is the reverse configuration to case 2. The results demonstrate that the Nafion gradient in the catalyst layer can play a significant role on the catalyst layer performance. Voltage losses are reduced by 3% at 0.8 A/cm$^2$ for case 2, in reference to the homogeneous case. For case 3 with the higher Nafion content near the GDL side, the voltage loss increases by 10% at 0.8 A/cm$^2$. The reason is straightforward as illustrated in Fig. 4b, which shows oxygen concentration profiles along the thickness coordinate at cell potential 0.6 V. Compared with the baseline case, case 2 exhibits a more homogeneous oxygen distribution throughout the catalyst layer; even though the oxygen concentration decreases fast in the sublayer on the membrane side, it is compensated by the increase of proton transport in this region. In case 3, a rapid decrease of the oxygen concentration is found in the catalyst layer near the GDL side. Due to the reduced rate of mass transfer, two thirds of catalyst layer operate under oxygen depletion.

Figure 5 shows comparisons of polarization curves for three and five sublayers. The results indicate no improvement by further subdivision of the catalyst layer for the favorable gradient with en-
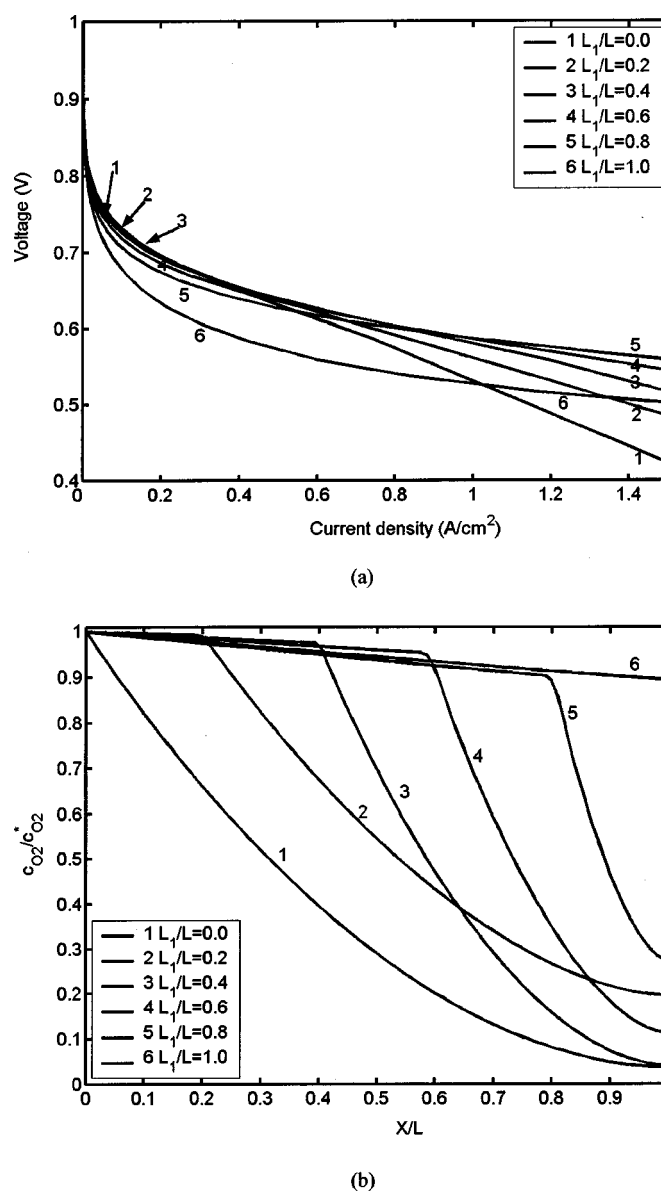


(a)



(b)

**Figure 6.** Performance dependence on Nafion weight fraction for a nonconstant Nafion gradient in the catalyst layer: (a) catalyst layer polarization relations and (b) oxygen concentration profiles at 0.6 V. (Nafion weight fraction: 25|40 %.)
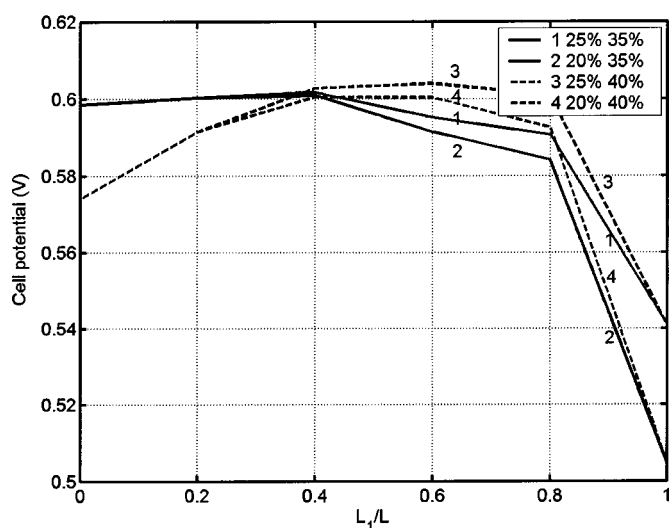
hanced $Y_{el}$ on the membrane side. However, the performance of five sublayers is improved slightly for the opposite case because the oxygen diffusion resistance is reduced.

*Nonconstant gradient.*—The two-sublayer structure with nonconstant composition gradient is shown in Fig. 1b. In the GDL side ($L_1$), the Nafion loading is varied from 20 to 25 wt %. In the membrane side ($L - L_1$), the Nafion loading is varied from 35 to 40 wt % and $L_1/L$ is varied from 0 to 1.

Figure 6 represents the polarization curves and the oxygen concentration profiles in the catalyst layer in which the Nafion weight fraction is 25 wt % on the GDL side and 40 wt % on the membrane side. It can be seen that the voltage losses increase at lower current density and decrease at high current density when $L_1/L$ is changed from 0 to 1, which means the thickness with 25 wt % of $Y_{el}$ increases. This behavior can be explained physically as follows: at low current density the rate of oxygen diffusion is sufficiently fast compared to the rate of electrochemical reaction; as a result, higher $Y_{el}$
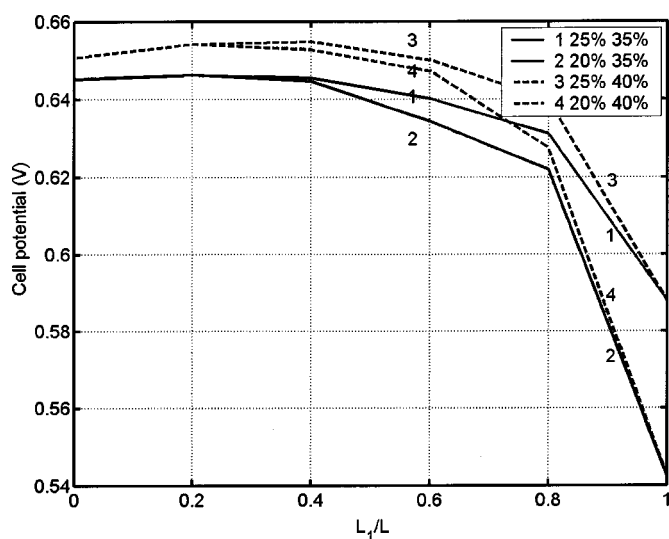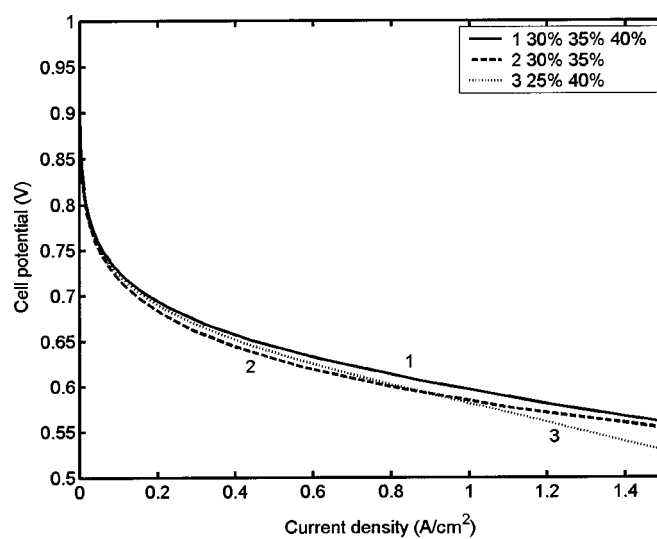
(a)



(b)

**Figure 7.** Cell potential with different $L_1/L$ at current density (a) 0.4 and (b) 0.8 A/cm$^2$.



(a)



(b)

**Figure 8.** Comparison of performance dependence on Nafion weight fraction in two- and three-sublayer structures of catalyst layers (two-sublayer $L_1/L = 0.5$): (a) polarization relations and (b) oxygen concentration profiles.
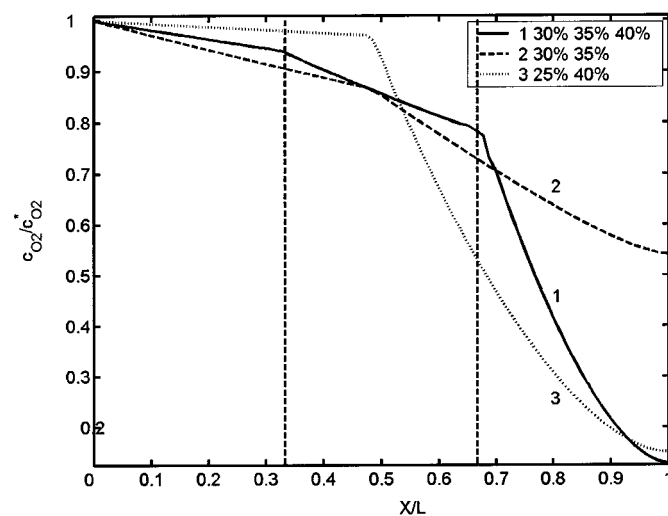
helps to increase the exchange current density and reduces voltage losses associated with proton transfer. A high cell current density consumes a large quantity of reactants, making oxygen supply the controlling process. Hence, a decrease in $Y_{el}$ is required for faster mass transfer of the reactant. Figure 6b shows the concentration profiles at cell voltage 0.6 V. It is found that with the $Y_{el}$ decrease, the oxygen concentration profiles get more uniform.

Figure 7 shows the cell potential with different $L_1/L$ and combination of Nafion gradients at current densities 0.4 and 0.8 A/cm$^2$. Within the limited number of considered cases, the highest cell potential is obtained at $L_1/L \approx 0.4$ for 0.4 A/cm$^2$ and at $L_1/L \approx 0.6$ for 0.8 A/cm$^2$. Compared to the baseline case with uniform Nafion loading 35 wt %, the cell potential could be increased by 3-5% at 0.4 A/cm$^2$ and by 1-2% at 0.8 A/cm$^2$.

Figure 8 presents the comparison of performance dependence on $Y_{el}$ in two- and three-sublayers of catalyst layer. It can be found that the three-sublayer design with Nafion gradient (30|35|40 wt %) has better performance than two-sublayer design (30|35 or 25|40 wt %).

## Conclusions

The dependence of oxygen diffusion coefficient, proton conductivity, ESA, and cathode performance on Nafion loading has been investigated. The model results reported in this paper indicate that an optimum Nafion content exists at 35 wt %. This finding is in accordance with experimental data in the literature.

The Nafion gradient for cathode catalyst layer has been demonstrated theoretically to have a significant influence on the cathode performance. Compared with the optimum Nafion content (35 wt %) in uniform distribution, a simple variation of Nafion loading with lower Nafion content (30 wt %) in the GDL side and higher Nafion content (40 %) in the membrane side could reduce the voltage losses in the catalyst layer by 3-5%. This is the way to improve the catalyst layer structure by optimizing both oxygen diffusion and proton transport.

Furthermore, potential advantages of this design are lower ohmic resistance in the interfaces and better water management. In the interface between GDL and CL, lower Nafion loading decreases the

probability of blockage of pores by Nafion and thereby facilitates water removal via the GDL. In the interface between CL and membrane, a higher Nafion loading increases the contact area between the electrolyte phases in the two media and thereby improves proton transport. Due to these effects, which are not considered in the present version of the model, even greater improvements in performance are expected with functionally graded catalyst layers.

Compared with constant Nafion gradient design in three-sublayer, nonconstant Nafion gradient with the two sublayers does not show much advantage in performance compared to the three sublayers; neither does a further subdivision into five or more sublayers.

Experimental evaluation of the model is currently underway and will be reported later. However, the preliminary experiments showed an agreement. Further refinements of the model will involve a more detailed structural picture based on the agglomerate model and consideration of the water balance in the electrode.

### Acknowledgment

### List of Symbols

| | |
|---|---|
| $A_s$ | the platinum surface area per unit mass of the platinum, $cm^2/mg$ |
| $c_{O_2}^*$ | oxygen concentration on the interface of GDL and catalyst layer, $mol/cm^3$ |
| $c_0^{ref}$ | oxygen reference concentration, $mol/cm^3$ |
| $c_{O_2,l}$ | dissolved oxygen concentration in electrolyte, $mol/cm^3$ |
| $c_{O_2}$ | oxygen concentration in the gas phase, $mol/cm^3$ |
| $D_{O_2}$ | bulk oxygen diffusion coefficient, $cm^2/s$ |
| $D_{O_2}^{eff}$ | effective oxygen diffusion coefficient in gas phase, $cm^2/s$ |
| $F$ | Faraday's constant, C/mol |
| $i_0^{ref}$ | reference exchange current density, $A/cm^2$ |
| $I_0$ | total current density, $A/cm^2$ |
| $j(x)$ | local proton current density, $A/cm^2$ |
| $K_{O_2}$ | oxygen Henry's constant |
| $L$ | catalyst layer thickness, cm |
| $L_1$ | thickness of catalyst sublayer, cm |
| $m_{Pt}$ | platinum loading in the catalyst layer, $mg/cm^2$ |
| $N_{O_2}$ | oxygen flux, $mol/(cm^2 s)$ |
| $R$ | gas constant, 8.314J/(mol K) |
| $S_a$ | catalyst specific area per unit volume, $cm^2/cm^3$ |
| $S_a^{eff}$ | effective catalyst specific area per unit volume, $cm^2/cm^3$ |
| $T$ | cell temperature, K |
| $X_0$ | percolation threshold |
| $X_C$ | volume portion of carbon phase |
| $X_{Pt}$ | volume portion of platinum phase |
| $X_{el}$ | volume portion of electrolyte |
| $X_V$ | volume portion of pore space |
| $Y_{Pt}$ | platinum mass fraction |
| $Y_{el}$ | mass fraction of electrolyte |

Greek

| | |
|---|---|
| $\rho_C$ | density of carbon black, $mg/cm^3$ |
| $\rho_{Pt}$ | density of platinum, $mg/cm^3$ |
| $\rho_{el}$ | density of electrolyte, $mg/cm^3$ |
| $\sigma_s$ | proton bulk conductivity, S/cm |
| $\sigma^{eff}$ | effective proton conductivity, S/cm |
| $\alpha_c$ | cathode transfer coefficient |
| $\eta(x)$ | local electrode potential, V |

### References

1. A. Damjanovic and J. O'M. Bockris, *Electrochim. Acta,* **11**, 376 (1961).
2. A. Damjanovic and V. Brusic, *Electrochim. Acta,* **12**, 615 (1967).
3. A. Damjanovic, in *Modern Aspects of Electrochemistry*, Vol. 5, J. O'M. Bockris and B. E. Conway, Editors, p. 369, Plenum Press, New York (1969).
4. A. J. Appleby, in *Modern Aspects of Electrochemistry*, Vol. 19, B. E. Conway and J. O'M. Bockris, Editors, p. 369, Plenum Press, New York (1974).
5. S. Gottesfeld, I. D. Raistrick, and S. Srinivasan, *J. Electrochem. Soc.,* **134**, 1455 (1987).
6. E. Parthasarathy, S. Srinivasan, and J. Appleby, *J. Electrochem. Soc.,* **139**, 2530 (1992).
7. P. D. Beattie, V. I. Basura, and S. Holdcroft, *J. Electroanal. Chem.,* **468**, 180 (1999).
8. M. Eikerling and A. A. Kornyshev, *J. Electroanal. Chem.,* **453**, 89 (1998).
9. Z. Poltarzewski, P. Staiti, A. Redondo, and S. Srinivasan, *J. Electrochem. Soc.,* **139**, 761 (1992).
10. E. Passalacqua, F. Lufrano, G. Squadrio, A. Patti, and L. Giorgi, *Electrochim. Acta,* **43**, 3665 (1998).
11. E. A. Ticianelli, J. G. Berry, and S. Srinivansan, *J. Appl. Electrochem.,* **21**, 597 (1991).
12. I. D. Raistrick, U.S. Pat. 4,876,115 (1989).
13. S. Srinivansan, E. A. Ticianelli, and C. R. Derouin, *J. Power Sources,* **22**, 359 (1988).
14. M. S. Wilson and S. Gottesfeld, *J. Appl. Electrochem.,* **22**, 1 (1992).
15. M. Uchida, Y. Aoyama, E. Eda, and A. Ohta, *J. Electrochem. Soc.,* **142**, 463 (1995).
16. M. Uchida, Y. Aoyama, E. Eda, and A. Ohta, *J. Electrochem. Soc.,* **142**, 4143 (1995).
17. V. A. Paganin, E. A. Ticianelli, and E. R. Gonzalez, *J. Appl. Electrochem.,* **26**, 297 (1996).
18. S. J. Lee, S. Mukerjee, J. McBreen, Y. W. Rho, Y. T. Kho, and T. H. Lee, *Electrochim. Acta,* **43**, 3693 (1998).
19. E. Antolini, L. Giorgi, A. Pozio, and E. Passalacqua, *J. Power Sources,* **77**, 136 (1999).
20. J. M. Song, S. Y. Cha, and W. M. Lee, *J. Power Sources,* **94**, 78 (2001).
21. F. A. Uribe and T. A. Zawodzinski, *Electrochim. Acta,* **47**, 3799 (2002).
22. S. C. Thomas, X. Ren, and S. Gottesfeld, *J. Electrochem. Soc.,* **146**, 4354 (1999).
23. E. Passalacqua, F. Lufrano, G. Squadrio, A. Patti, and L. Giorgi, *Electrochim. Acta,* **46**, 799 (2001).
24. M. Eikerling and A. A. Kornyshev, *J. Electroanal. Chem.,* **475**, 107 (1999).
25. M. Eikerling, A. A. Kornyshev, and A. A. Kulikovsky, in *Encyclopedia of Electrochemistry*, Vol. 5, *Electrochemical Engineering*, D. D. Macdonald, Editor, To be published.
26. R. P. Iczkowski and M. B. Cutlip, *J. Electrochem. Soc.,* **127**, 1433 (1980).
27. S. J. Ridge, R. E. White, Y. Tsou, R. N. Beaver, and G. A. Eisman, *J. Electrochem. Soc.,* **136**, 1902 (1989).
28. D. M. Bernardi and M. W. Verbrugge, *AIChE J.,* **37**, 1151 (1991).
29. T. E. Springer, M. S. Wilson, and S. Gottesfeld, *J. Electrochem. Soc.,* **140**, 3513 (1993).
30. C. Marr and X. Li, *J. Power Sources,* **77**, 17 (1999).
31. M. Mezedur, M. Kaviany, and W. Moore, *AIChE J.,* **48**, 15 (2002).
32. J.-H. Nam and M. Kaviany, *J. Heat Mass Transfer,* **46**, 4595 (2003).
33. J. M. Hammersley, *Proc. Cambridge Philos. Math. Phys. Sci.,* **53**, 642 (1957).
34. A. Ioselevich, A. A. Kornyshev, and W. Lehnert, *Solid State Ionics,* **124**, 221 (1999).
35. D. Stauffer and A. Aharony, *Introduction to Percolation Theory*, Rev. 2nd ed., Taylor and Francis, London (1994).
36. M. B. Isichenko, *Rev. Mod. Phys.,* **64**, 961 (1992).
37. S. Feng, B. I. Halperin, and P. N. Sen, *Phys. Rev. B,* **35**, 197 (1987).
38. S. J. Chapman, *MATLAB Programming for Engineers*, Pacific Grove, CA (2002).